TRANSFORMATION OF SINGULAR JOINT DEFORMATIONS INTO MULTIPLE CRACKS IN CARBON REINFORCED CONCRETE PAVEMENTS

MAXIMILIAN WEIß[*] AND IURIE CUROȘU[*]

[*] Ruhr-University Bochum, Chair of Construction Materials
Universitätsstraße 150, 44801 Bochum, Germany
e-mail: Maximilian.Weiss-j1i@rub.de, www.baustoffe.ruhr-uni-bochum.de

Key words: Carbon-Reinforced Concrete, Ductile Joint Overbuild, Concrete Pavements, Image-Based Crack Detection

Abstract: Large concrete surfaces in industrial and parking areas, roads or highways, are typically designed with joints to mitigate constraint-induced stresses and uncontrolled crack formation. Thermal or hygric concrete deformations localize at these joints, which can vary in thickness from a few millimeters to several centimeters. To prevent the ingress of harmful substances into the concrete and its substrate, joints are typically sealed by flexible polymer sealants. However, the durability of these sealing systems is limited, despite being regularly maintained. Furthermore, the concrete in the joint areas often yields premature damage under combined mechanical loads and environmental exposures.

This paper presents an alternative concept consisting in overbuilding existing joints with a thin layer of carbon reinforced concrete (CRC). The CRC layers transform the joint deformations into multiple fine cracks over a predefined area, enabling an extended service life an enhanced traffic comfort. The work deals with the design of a large-scale testing facility including initial reference experiments on CRC joint systems. The experimental setup was developed to simulate both positive and negative, quasi-static and cyclic joint deformations at a full scale. It allows deriving the mechanical response of the system and analyze the damage development and crack formation by means of analogue and image-based techniques

1 INTRODUCTION

Concrete pavements are subjected to mechanical stresses from traffic loads, as well as thermal and hygric stresses induced by varying climatic conditions.

Weather fluctuations, both seasonal and diurnal, create temperature and moisture gradients, leading to constrained stresses and deformations. Depending on the loading scenario, these may manifest as longitudinal or transversal compressive stresses, as well as tensile or flexural stresses. Without proactive measures, extensive cracking and spalling of the concrete pavement can occur, significantly impairing its functionality and allowing pollutants to infiltrate, which reduces its durability.

One strategy to address this issue is to reinforce the concrete slabs by steel rebars, in this way also ensuring an adequate crack control. However, due to the significant amount of reinforcement this method might not always prove economical.

A common approach for concrete pavements with minimum or no reinforcement is the implementation of Jointed Plain Concrete Pavements (JPCP). These pavements incorporate joints designed to act as fracture

planes to prevent the formation of extensive cracks and allow for unrestrained expansion during slab deformations. To mitigate the infiltration of harmful liquid pollutants and debris, joint sealing compounds or joint profiles are utilized. Nonetheless, the limited durability of these joint sealants poses a challenge, necessitating periodic maintenance or replacement at intervals of 5-10 years [1]. The maintenance or repair of joint sealing entails supplementary expenses and may temporarily disrupt the functionality of the roadway. Thus, while joints serve as essential construction components, they also represent vulnerabilities in concrete pavements. Therefore, there is need for an alternative joint repair concept that, in addition to low-maintenance functionality, also meets the durability expectations.

2 FAILURE MECHANISMS IN CRC

Thin concrete overlays are already being used as repair measures in several areas [2]. Building on this, initial methods using carbon-reinforced concrete were developed [3], [4] and have since undergone continuous refinement.

Both carbon and steel reinforcement involve three main bonding mechanisms, adhesion, friction and mechanical interlock [5], [6], [7], [8]. At larger interfacial displacements, the adhesive bond is exceeded, and the frictional bond is activated. Depending on the rebar or roving profile, the interlock can have a major or only a minor contribution to the anchorage of the reinforcement. Initially, carbon and steel exhibit very similar behavior in the uncracked state (State I). However, a significant difference between the reinforcement materials emerges at large deformations, i.e. during cracking in State II. At this stage, steel reinforcement demonstrates a pronounced yielding and high plastic deformability, whereas carbon reinforcement exhibits a linear elastic response up to failure [9].

As opposed to ordinary reinforced concrete, in which the rebar yielding defines a limit state, in CRC the limit state is rather defined by safety factors attributed to the tensile strength of the yarns. It is however common, that the strains in the yarns upon reaching a certain limit state are several times larger as those corresponding to the yielding initiation of the rebars.

In CRC overlays it is necessary to transform the joint opening into a smeared deformation by inducing a multiple cracking in the concrete and at the same time avoiding damage initiation in other regions, such as in the substrate. An extensive exploitation of the yarn tensile strain capacity is adequate if the induced damage is controlled.

A typical failure mode in CRC is related to the yarns themselves and it depends on the coating or impregnation. A "soft" or insufficient impregnation leads to a weak load redistribution among the individual filaments, which leads to a telescopic yarn failure. A "stiff" impregnation leads to a sudden localized rupture of the yarn. Also, upon an insufficient anchorage, the yarns are pulled out of the concrete. Finally, a pronounced yarn deformation can lead to pronounced out-of-plane stresses and delamination of the concrete cover along the plane mesh [5], [7], [8], [10]. Further failure mechanisms relate to the entire system, i.e. between the CRC overlay a concrete substrate, or even pronounced cracking in the substrate itself due to tensile and flexural stresses induced by the tensioned CRC. Thus, the design of such overlays requires a holistic consideration of the entire system and experimental investigations at a representative scale additionally to the tests on separate components.

3 CRC FOR JOINT OVERBUILDS

Preliminary methodologies using carbon reinforcement have been explored for the rehabilitation of steel-reinforced concrete structures. However, these methods are primarily limited to mortar applications and are typically associated with scenarios involving lower levels of crack movement and low-cycle loading [11].

Carbon reinforcement provides superior

elastic deformability and corrosion resistance compared to steel reinforcement, which allows achieving ductile and durable overlays with small thicknesses. With common mesh geometries CRC also yields a superior crack control in terms of spacing and width. This is in contrast to steel-reinforced concrete pavements, which generally develop fewer but wider cracks.

The procedure discussed here involves applying a thin layer of CRC ranging from 40 mm to 70 mm over the joints. The entire overlay system including the concrete substrate is presented in Figure 1. One of the goals of this study was thus to design and build a setup that allows testing the entire system at a representative scale but under laboratory conditions.
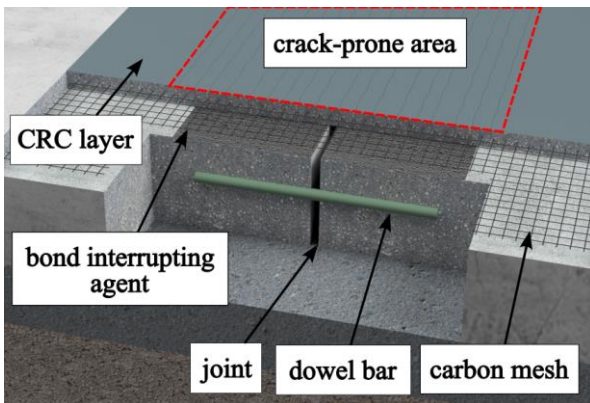
Figure 1: Schematic illusration of a CRC joint overbuild with sectional view of the JPCP

4 EXPERIMENTAL INVESTIGATIONS

The intended setup should allow to develop a fundamental understanding of the deformation behavior and cracking mechanisms as well as induced stresses in CRC layers with the concrete substrate and overlayed joints. This study focuses on analyzing how localized joint deformations are distributed into numerous microcracks within the CRC layer without negatively affecting the thickness of the system and traffic safety.

The systematic study involving various carbon reinforcements, reinforcement degrees, layer thicknesses and overlay-substrate bonding properties, should provide the basis for further adjustments and finally the formulation of design criteria of CRC for this specific application.

4.1 Materials and compositions

The specimens tested in this study consist of a bottom concrete layer, which simulates the old concrete pavement (JPCP), and an overlay of CRC, for which a separate mix design was developed. The JPCP was composed of a standard road concrete mix conforming to the German guideline TL Beton-StB 07 [12]. The specifications require a concrete of strength class C30/37, exposure class XF4, with a maximum aggregate size of 22 mm, moisture class WS, and a minimum cement content of 420 kg/m³. For the CRC layer, a standard road concrete mix was selected and subsequently modified (see Table 1). This modification aimed to achieve a higher consistency class F4, maintain a minimum average air void content of 5.5 Vol.-%, and limit the maximum aggregate size to 8 mm, in this way ensuring compatibility with the mesh size of the carbon reinforcement.

Table 1: Concrete compositions

Materials		CRC	JPCP
Cement		430	340
Sand 0/2		516	544
Basalt 2/5	[kg/m³]	634	168
Basalt 5/8		634	168
Basalt 8/16		-	440
Basalt 16/22		-	774
Superplasticizer	[M.-%$_{Cem}$]	0.70	0.42
Air-entraining agent	[M.-%$_{Cem}$]	0.20	0.20
w/c	[-]	0.42	0.45

Two different types of carbon textiles were selected for the CRC layer, differing in their geometric and mechanical properties. The meshes used are the GRID Q85-CCE-21 from Solidian® and the SITgrid 041 KK from Wilhelm Kneitz® [13], [14]. The selection was based on the compatibility of the mesh opening with the maximum aggregate size, as well as appropriate in-plane load distribution within the CRC layer. The properties of the carbon textiles used are shown in Table 2.

3

Table 2: Properties of the carbon textiles

Parameter		SITgrid 041 KK	GRID Q95
Coating		PU	Epoxy
Yarn cross-sectional area	[mm²/m]	70.5	95.0
Yarn spacing	[mm]	23.0	34.0
Tensile strength	[MPa]	~2500	~3910
Elongation at fracture	[%]	1,0[1]	1,2[2]

[1][15] [2][16]

4.2 Specimens

For the experimental studies, beam-shaped test specimens were designed to simulate a typical concrete roadway. The test specimens consist of a bottom concrete layer, which replicates JPCP, and a top concrete layer made of CRC (see Figure 2). The bottom concrete specimen consists of two symmetrically arranged blocks with dimensions of 620 mm x 300 mm x 100 mm (L x W x H). The joint in the substrate is simulated by a 10 mm gap between the concrete blocks. A smooth stainless steel dowel bar (d = 20 mm) is positioned in the center of the cross-section at the end faces adjacent to the joint. The dowel bar is housed in plastic dowel sleeves.

Two threaded sleeves are positioned at the outer ends of the specimen, which are used to secure the specimen within the test frame and apply the load during the test. Both anchor sleeves are equipped with a structural reinforcement bracket, which ensures anchoring in the bottom concrete specimen. Similarly, the anchor sleeves are centered in the cross-section of the bottom concrete specimen (h = 50 mm).
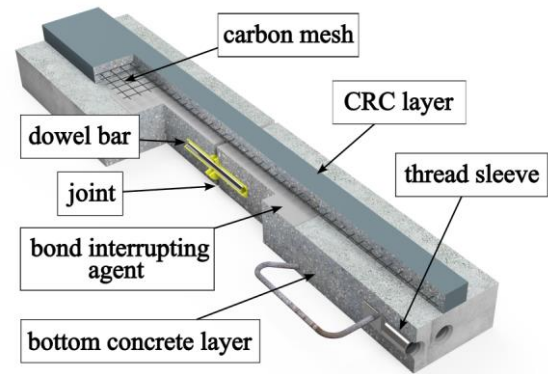
Figure 2: Sectional view of the specimen

The surface of the substrate is treated with a retarder immediately after concreting and then rinsed to obtain an exposed aggregate structure. This roughened surface is necessary to ensure a sufficient bond with the applied CRC layer in the designated areas and replicate the practical execution of such systems on site. In the joint entry area, where the development of finely distributed cracks in the CRC layer is anticipated, substrate is coated with a bond interrupting agent, in this case consisting of bitumen. The isolated bond-free area must primarily facilitate shear and tensile relative displacements between the bottom and top concrete layers and serve as a free length for crack development in the CRC.

4.3 Test Setup

Due to the cyclic joint deformations, varying stress states develop in the applied CRC layer. These stresses can be induced both by moisture and temperature variations, and they are subject to short-term (day-night) and long-term (summer-winter) cycles.

To investigate this, a horizontally aligned test rig was constructed in accordance with the Federal Waterways Engineering and Research Institute (BAW) data sheet, albeit with modified dimensions and test procedures [17]. The foundation of the test rig is a stiff frame made of steel profiles (see Figure 3). The test specimen is placed on a low-friction base and the fixed end is secured of the frame using screw connections in threaded sleeves set in concrete. On the opposite side, the test specimen is connected to a hydraulic cylinder.

This double-acting hydraulic cylinder has a compressive force capacity of 150 kN and a tensile force capacity of 100 kN. It operates under displacement control at a constant speed of 1 mm/min. The setup allows for both static tension and compression tests, as well as cyclic tests. The force and position of the hydraulic cylinder are continuously recorded. Additionally, the movement of the joint (opening and closing) in the test specimen is measured using four laser distance sensors, with two sensors positioned on each side.
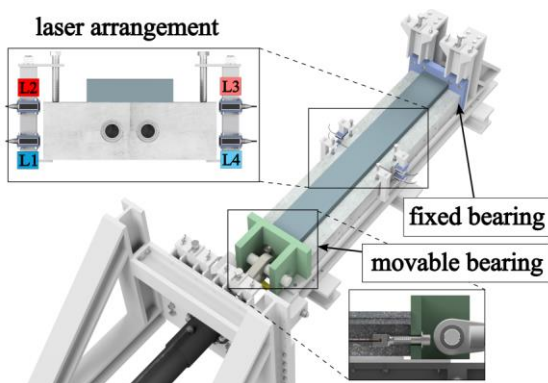
Figure 3: Testing frame with detail view of the load introduction and arrangement of the displacement sensors

5 RESULTS AND DISCUSSION

The following section presents the results of two test runs conducted with two distinct test specimens, which vary in reinforcement mesh, number of reinforcement layers, and thickness of the CRC layers. Various testing parameters were recorded, including cylinder force, cylinder displacement, and in-plane joint displacement. Additionally, the CRC layer was photographed using a conventional high-resolution camera. The captured images underwent several processing steps to identify cracks in the CRC layer by analyzing differences in the grayscale values of the image pixels. Subsequently, this analysis facilitated the monitoring of crack widths throughout the test duration. By employing a reference scale within the images, the crack width in millimeters was determined based on the pixel count within a crack.

The tests were terminated as soon as an increase in the joint opening of 10 mm was

reached or the test specimen failed prematurely. The joint opening defined as the burn-off criterion was determined based on a dimensioning commonly used in practice [1].

5.1 Specimen A

Specimen A was fabricated using a single reinforcement layer of GRID Q95-CCE-38 embedded within a 40 mm thick layer of concrete and 20 mm of concrete cover (reinforcement ratio = 0.13 %).

Figure 4 illustrates the temporal progression of tensile forces and joint movements for Specimen A. The formation of four cracks is discernible from the data, indicated by a transient application of tensile force and a sudden increase in joint opening. Over the course of the test, a pronounced increase in joint opening was recorded by lasers 1 and 4, in contrast to the other lasers. These lasers are positioned at the bottom edges of the joint (refer to Figure 3), suggesting an upward movement of the specimen half on the movable bearing side, thereby indicating the development of a bending moment within the joint. The loading was stopped upon reaching 10 mm joint opening, as derived by laser 1. A maximum tensile force of 21.2 kN was measured. This corresponds to a stress in the reinforcement of around 1.470 N/mm².
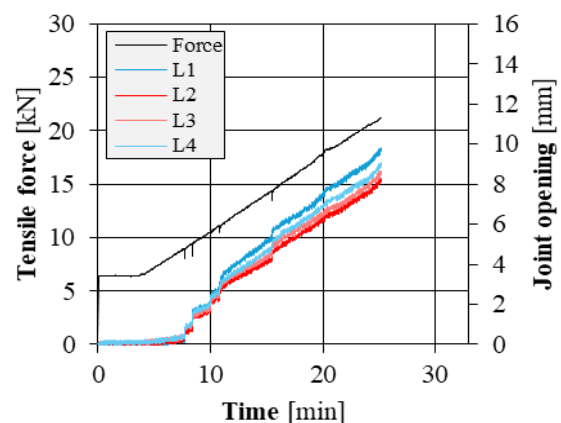
Figure 4: Tensile force progression and joint movement (specimen A)

Additionally, Figure 5 presents the top view of the CRC layer of Specimen A. The region where the CRC layer overlays the joint is highlighted in red. The area previously treated

with a bond breaker (length = 600 mm) is delineated with a dashed frame. The figure also indicates the positions of the cracks and the chronological sequence of their formation.
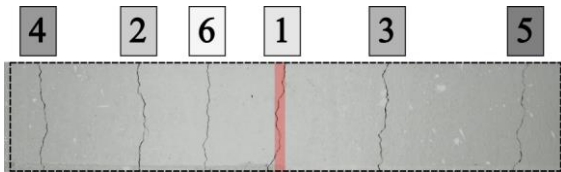
Figure 5: Top view of the crack area (specimen A)

A total of six cracks developed in the CRC layer by the conclusion of the test. The initial cracks predominantly appear adjacent to the joint, whereas subsequent cracks tend to manifest within the isolated bond-free region. The average spacing between the cracks is 13.1 cm.

Furthermore, Figure 6 illustrates the temporal progression of the average crack widths in relation to the tensile force. Cracks 2 through 6 exhibit a similar trend, characterized by a rapid increase followed by a deceleration in the crack opening rate upon the formation of a new crack. In contrast, the progression of crack 1 demonstrates significant stiffening at an average crack opening of 0.4 mm prior to the load ascent, likely indicating pre-damage to the specimen due to storage conditions. Overall, all crack openings at the conclusion of the test remain below 0.9 mm, with an average joint opening of approximately 9 mm (refer to Figure 4).
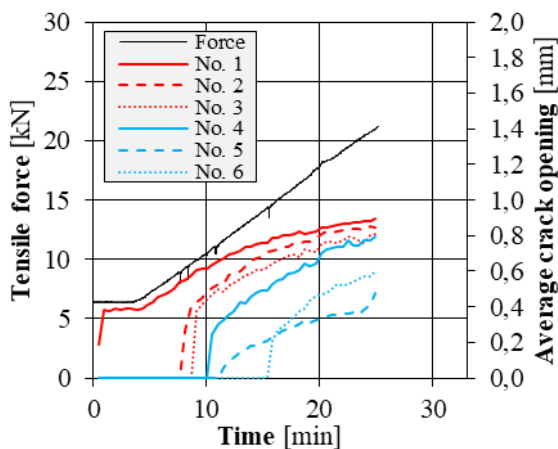
Figure 6: Temporal progression of tensile force and crack opening development (specimen A)

5.2 Specimen B

Test specimen B was constructed with three layers of SITgrid 041 KK reinforcement, embedded in a 70 mm-thick carbon concrete layer. Spacers were used to maintain a 20 mm distance between the reinforcement layers and to ensure a concrete cover of 15 mm (reinforcement ratio = 0.31 %). In Figure 7, the joint movements and tensile forces are illustrated analogous to those of specimen A.

The test had to be prematurely terminated at a tensile force of approximately 29 kN due to the appearance of a failure indicator, specifically a horizontal crack in the bottom concrete block at the point of load application (thread sleeve). This corresponds to a stress in the reinforcement of around 890 N/mm². The maximum joint movement recorded up to this load level was about 6.5 mm (L4). Additionally, an unexpected deviation in the curve was observed due to the unscheduled loosening of the support for laser 1 during the test.
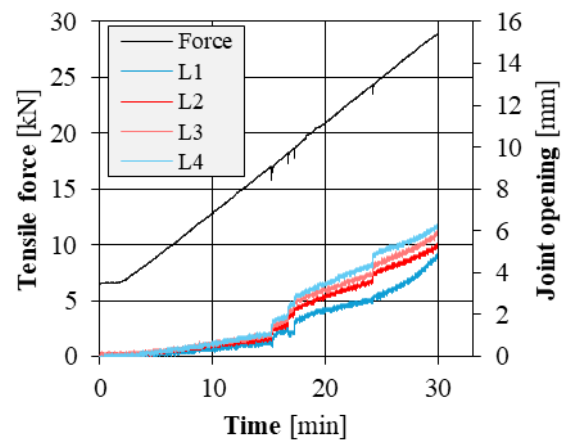
Figure 7: Tensile force progression and joint movement (specimen B)

Furthermore, Figure 8 illustrates the cracking pattern of the deck shortly before the test ended. Similar to the crack pattern of specimen A, the initial crack in this case also occurs in the immediate area of the joint. The formation of the remaining cracks, however, follows no discernible pattern but is rather evenly distributed across the zone of bond separation. The average distance between the cracks is 12.5 cm, which is comparable to that

observed in specimen A.
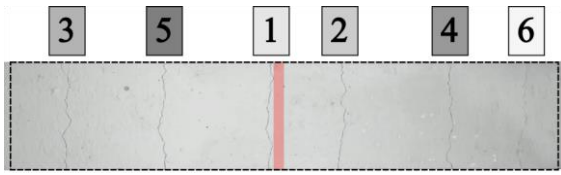
Figure 8: Top view of the crack area (specimen B)

Figure 9 illustrates the average crack opening over time for specimen B. The progression of crack number 6 is not depicted here, as it is presumed that the contrast at the crack edge was too low for effective image-based crack detection. Observing the progression of crack widening, a similar, almost linear increase is evident for all cracks. At the end of the test, the mean crack openings ranged between 0.35 mm and 0.45 mm. It is plausible to suggest that both the linear increase in mean crack openings and the narrower crack widths (despite the premature termination of the test) are directly attributable to the higher degree of reinforcement.
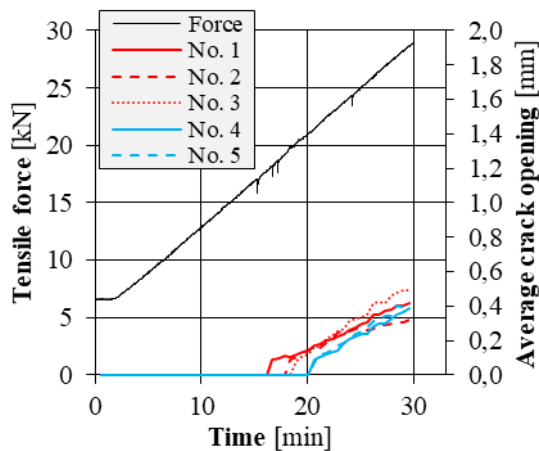
Figure 9: Temporal progression of tensile force and crack opening development (specimen B)

6   CONCLUSIONS AND OUTLOOK

Based on initial tensile evaluations conducted on large-format specimens, the development of cracks within thin-layer overlays composed of carbon-reinforced concrete was preliminarily explored using a dedicated experimental setup. Using a specialized testing apparatus, specific types of cracks can be induced within the CRC matrix,

facilitating concurrent analyses via image-based measurements. This methodology enables the assessment of crack progression, as well as the temporal evolution of crack widths and spacings.

In terms of crack behavior, both examined specimens exhibited a generally similar crack pattern despite differences in the configuration of the CRC layer. This similarity in crack patterns is particularly evident in the number of cracks and their average spacing. The essential differences were observed in the progression of crack openings. For example, the cracks in Specimen A exhibited a sharp increase in width, which then plateaued, whereas the cracks in Specimen B demonstrated a consistent linear expansion from the outset. Additionally, these cracks had a more uniform size distribution and were generally narrower compared to those in Specimen A. However, it is important to note that the testing was limited to a joint opening less than 10 mm due to a failure in the load introduction mechanism of specimen B. Consequently, a comparison of the crack widths is possible only to a limited extent.

For image-based crack analysis, maintaining a consistent distance between the camera and the specimen, along with uniform lighting conditions during the capture process, is crucial. This approach can reduce the processing effort of the video material and enhance the precision of crack detection.

These preliminary experiments demonstrate the necessity of a systematic experimental study on a realistic scale. The overlay system implies a variety of possible damage patterns and failure modes, which have to be detected and controlled. The ongoing studies will thus focus on these aspects involving additionally different loading conditions, geometric configurations and reinforcement types. To widen the set of analyzed parameters and allow for an isolated analysis of the decisive mechanisms, complementary Finite Element simulations with a discrete reinforcement representation are carried out.

8 REFRRENCES

[1] Road and Transportation Research Association (FGSV), 2015. ZTV Fug-StB 15, Zusätzliche Technische Vertragsbedingungen und Richtlinien für Fugen in Verkehrsflächen.

[2] Morales Cruz, C., Raupach, M., 2014. Untersuchungen zur kontrollierten Rissverteilung textilbewehrter Schutzschichten mit optischer 3D-Verformungsanalyse. Restoration of Buildings and Monuments 20, vol. 5:299–310.

[3] Feix, J., Hansl, M., 2012. Zur Anwendung von Textilbeton für Verstärkungen im Brückenbau. Festschrift zum 60. Geburtstag von Univ.-Prof. Dr.-Ing. Manfred Keuser, Berichte aus dem konstruktiven Ingenieurbau 12(4):289–295. Universität der Bundeswehr, München.

[4] Hansl, M., 2014. Textilbewehrte Betone zur Instandsetzung und Verstärkung von Fahrbahnplatten aus Stahlbeton. Diss., Leopold-Franzens-Universität, Innsbruck.

[5] Schütze, E., Curbach, M., 2019. Zur experimentellen Charakterisierung des Verbundverhaltens von Carbonbeton mit Spalten als maßgeblichem Versagensmechanismus. Bauingenieur 94, vol. 4, 133–141.

[6] Lorenz, E., 2014. Endverankerung und Übergreifung textiler Bewehrung in Betonmatrices. Faculty of Civil Engineering, Dresden University of Technology, Ph.D. Thesis, Dresden.

[7] Bielak, J., Spelter, A., Will, N. and Classen, M., 2018. Verankerungsverhalten textiler Bewehrungen in dünnen Betonbauteilen. Beton- und Stahlbetonbau 113, vol. 7: 543–550.

[8] Preinstorfer, P., Kromoser, B. and Kollegger, J., 2019. Kategorisierung des Verbundverhaltens von Textilbeton. Bauingenieur 94, vol. 12:416–424.

[9] Weiland, S., 2009. Interaktion von Betonstahl und textiler Bewehrung bei der Biegeverstärkung mit textilbewehrtem Beton. Faculty of Civil Engineering, Dresden University of Technology, Ph.D. Thesis, Dresden.

[10] Preinstorfer, P., Kromoser, B. and Kollegger, J., 2018. Einflussparameter auf die Spaltrissbildung in Textilbeton. Beton- und Stahlbetonbau 113, vol. 7:515–524.

[11] Breitenbücher, R., Neumann, J., 2020. C3-V4.12 Instandsetzung von geschädigten Betonfahrbahndecken mit Carbonbeton. Abschlussbericht Teilprojekt V4.12-I: Verbundverhalten unter Ermüdungsbeanspruchung. Bundesministerium für Bildung und Forschung (BMBF).

[12] Road and Transportation Research Association (FGSV), 2007. TL Beton-StB 07, Technische Lieferbedingungen für Baustoffe und Baustoffgemische für Tragschichten mit hydraulischen Bindemitteln und Fahrbahndecken aus Beton.

[13] Solidian GmbH, 2023. Technical Data Sheet for Textile Reinforcement (GRID Q95-CCE-38 F01R01).

[14] Wilhelm Kneitz Solutions in Textile GmbH, 2024. Technical Data Sheet for Textile Reinforcement (SITgrid 041 KK).

[15] Kim, H.-Y.; You, Y.-J.; Ryu, G.-S.; Ahn, G.-H.; Koh, K.-T. Concrete Slab-Type Elements Strengthened with Cast-in-Place Carbon Textile Reinforced Concrete System. Materials 2021, 14, 1437.

[16] Curbach, M., Frenzel, M., 2023. C3-V4.12 Zwanzig20 Carbon Concrete Composite - C³; Verbundprojekt 3.1: Ergebnishaus des C-Projektes – CUBE; Teilprojekt 1: Weiterentwicklung, Untersuchung und Nachweisführung von Bauteilen und Tragwerken aus Carbonbeton sowie wissenschaftliche Begleitung von Entwurfs-, Konstruktions- und Bauüberwachungsprozessen im Carbonbetonbau. Bundesministerium für Bildung und Forschung (BMBF).

[17] Bundesanstalt für Wasserbau (BAW), 2019. Merkblatt Flächige Instandsetzung von Wasserbauwerken mit textilbewehrten Mörtel- und Betonschichten (MITEX).